CHEMICAL ENGINEERING TRANSACTIONS
VOL. 127, 2026
A publication of AIDIC
The Italian Association of Chemical Engineering
Online at www.cetjournal.it
Guest Editors: Laura Capelli, Marzio Invernizzi, Selena Sironi

**ISBN** 979-12-81206-28-1; **ISSN** 2283-9216
DOI: 10.3303/CET26127004

# CFD-based Characterisation and Validation of Hydrogen-Sulphide Emissions in a Micro-Chamber/Thermal Extractor

Bruno Furieri[a], Laíze Nalli de Freitas[a,*], Thais Nunes Guerrero[b], Ademir Abdala Prata Jr.[c], Ruth Fisher[b], Richard Stuetz[b], Jane Meri Santos[a], Neyval Costa Reis Junior[a]

[a]Federal University of Espírito Santo
[b]University of New South Wales
[c]São Paulo State University
laize.freitas@edu.ufes.br

New analytical technologies for measuring trace atmospheric pollutants are being introduced every year in the search for easier pollutant quantification. One example, already applied in some European countries, is the Micro-Chamber/Thermal Extractor ($\mu$-CTE250), also known as the "Micro-chamber", a compact emission-analysis system whose main advantages are the small sample volume required, the low carrier-gas flow rate, and the rapid results. However, these emerging technologies still lack thorough validation and standardized operating protocols.
The present study proposes the use of Computational Fluid Dynamics (CFD) simulations to characterize the internal flow and mass-transfer mechanisms, as well as to quantify local and global mass-transfer coefficients of hydrogen sulfide ($H_2S$) inside the device. A three-dimensional model of a single stainless-steel slot chamber (57 mm diameter, 14 mm height, 15 mL liquid) was built in ANSYS Fluent. The carrier gas ($N_2$, 50 mL $\mathrm{min}^{-1}$) yields a Reynolds number of 22.8; therefore, the flow was solved as laminar and incompressible. Model outputs will be validated against independent decay experiments conducted at 21 and 30 °C. The resulting CFD framework will support future calibration of micro-chambers, guide protocol development, and improve emission-factor estimates for quiescent wastewater sources.

## 1. Introduction

The quantification of emissions of air pollutants from diffuse sources is based on methodologies that are both well established and widely explored in the scientific literature. A range of approaches are used for estimating emissions, each offering different advantages and limitations (Carrera et al., 2025). These methodological variations reflect the complexity and heterogeneity of diffuse emission sources (Liu et al., 2023; Monster et al., 2019), which often lack clear spatial boundaries and exhibit significant temporal variability. Consequently, selecting an appropriate estimation technique requires careful consideration of the emission context, measurement constraints, and the desired level of precision. Advancements in experimental setups, such as micro-scale chambers, together with the integration of modeling tools, have contributed to improving the reliability of these estimations.
Since the mid-2000s, micro-scale flux devices such as the Micro-Chamber/Thermal Extractor (μ-CTE) have emerged as promising alternatives to conventional flux hoods for measuring gaseous emissions. The standard μ-CTE has a small headspace volume, only 0.11 L ($1.14 \times 10^{-4}$ m³), and offers precise control over experimental parameters such as temperature, humidity, and air exchange rate. It features four independent cells mounted on a single heating block, enabling parallel processing of multiple replicates. By reducing the enclosed volume by two to three orders of magnitude compared to a US EPA dynamic flux chamber (DFC), the μ-CTE significantly shortens equilibration times from hours to minutes, requires only gram-scale samples, and can operate in a typical temperature range of 40 to 120 °C.

Paper Received: 12 March 2026; Revised: 12 May 2026; Accepted: 2 June 2026
Please cite this article as: Furieri B., Nalli de Freitas L., Nunes Guerrero T., Prata Jr. A.A., Fisher R., Stuetz R., Santos J.M., Reis Junior N.C., 2026, CFD-based Characterisation and Validation of Hydrogen-Sulphide Emissions in a Micro-Chamber/Thermal Extractor, Chemical Engineering Transactions, 127, 19-24 DOI:10.3303/CET26127004

Despite its increasing adoption, the µ-CTE still lacks inter-laboratory validation and established normative guidelines. While several case studies have demonstrated high efficiency and precision (De Baerdemaeker and Van Overmeiren, 2024; Wang et al., 2021; Kamarulzaman et al., 2019), there is currently no universal correction factor comparable to the rescaling equations proposed for the USEPA DFC.
As a result, each research group must independently calibrate its own device. Moreover, direct comparisons with standard methods such as portable wind tunnels or DFCs under real field conditions remain scarce, particularly for complex and heterogeneous sources.
Building on these findings, there is a clear need for a more in-depth investigation of the micro-chamber method, with the goal of elucidating the mass transfer mechanisms that take place within the device. To address this, the present study proposes the use of numerical simulations to characterize the internal distribution of concentration gradients. The insights gained from this analysis are expected to support the future validation of the apparatus and enhance its application in emission quantification.

## 2. Methodology

The flow and species transport were modeled using the governing equations of mass conservation (Equation 1), momentum conservation (Equation 2), and species transport (Equation 3). These equations describe the transient behavior of an incompressible fluid.

$$\frac{\partial \rho}{\partial t} + \nabla \cdot (\rho u) = 0 \quad (1)$$

$$\frac{\partial (\rho u)}{\partial t} + \nabla \cdot (\rho u u) = -\nabla p + \nabla \cdot [(\mu + \mu_t)(\nabla u + (\nabla u)^T)] + \rho g \quad (2)$$

$$\frac{\partial (\rho C)}{\partial t} + \nabla \cdot (\rho u C) = \nabla \cdot [(\Gamma + \Gamma t)\nabla C], \; \Gamma_t = \frac{\mu_t}{Sc_t} \quad (3)$$

where ρ is the fluid density [kg/m³], u is the velocity vector [m/s], p is the pressure [Pa], µ is the dynamic viscosity [Pa·s], $\mu_t$ is the eddy viscosity [Pa·s], g is the gravitational acceleration [m/s²], C is the mass concentration of hydrogen sulfide [kg/m³], Γ is the molecular diffusivity [m²/s], $\Gamma_t$ is the turbulent diffusivity [m²/s], and $Sc_t$ is the turbulent Schmidt number [-]. The computational domain was based on the µ -CTE 250 geometry (Figure 1 and Table 1). Figure 2 shows a schematic representation of the constructed geometry, including the Petri dish location and the gas inlet and outlet interfaces. The computational domain was discretized using an unstructured mesh composed of 2,494,999 elements.
The flow was characterized as laminar (Re ≈ 0.46) and transient. Species transport was modeled using the Mixture model, considering air as the primary fluid and a mixture of air and hydrogen sulfide ($H_2S$) as the transported species. Boundary conditions were defined as follows: a velocity inlet with a uniform air velocity of $5.19 \times 10^{-6}$ m/s, no-slip condition at all solid walls, and a pressure outlet set to zero-gauge pressure.

*Table 1: Geometric and flow parameters used in the CFD model of the micro-chamber, based on the actual dimensions of the µ-CTE250 experimental device.*

| Microchamber parameter | Value |
|---|---|
| Depth | 3.60E-02 m |
| Internal diameter | 6.40E-02 m |
| Outlet diameter | 5.00E-03 m |
| Inlet velocity | 2.36E-03 m/s |
| Petri dish area | 2.55E-03 m |
| Petri dish height | 5.88E-03 m |
| Reynolds number | 0.46 |

The emission profile of $H_2S$ was prescribed based on experimental decay data obtained from laboratory measurements of the liquid and gas phase (Figure 3). Two isothermal temperature cases were simulated: 21°C and 30°C, assuming constant temperature throughout the domain during each simulation.
ANSYS Fluent version 19.1 was used, with a transient formulation based on the first order implicit time- stepping scheme. Pressure–velocity coupling was handled using the SIMPLE (Semi-Implicit Method for Pressure- Linked Equations) algorithm, suitable for incompressible and weakly compressible flows (ANSYS Inc., 2023). For spatial discretization, the Least Squares Cell-Based method was employed.

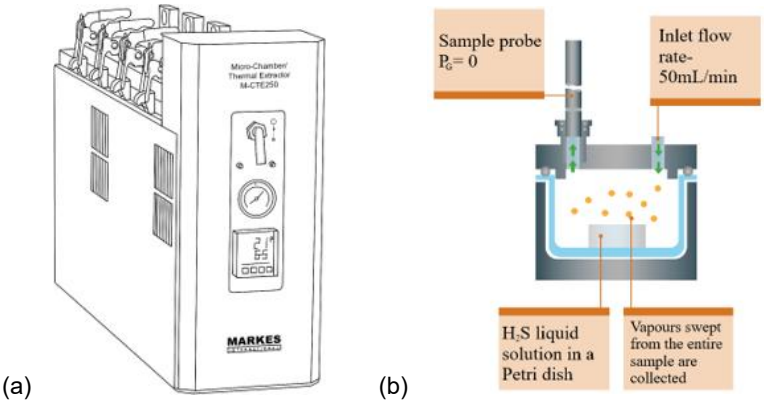


(a) (b)

*Figure 1: (a) Schematic of the micro-camera used in outline; (b) and diagram of the inside of a micro-camera slot, detailing the sampling.*

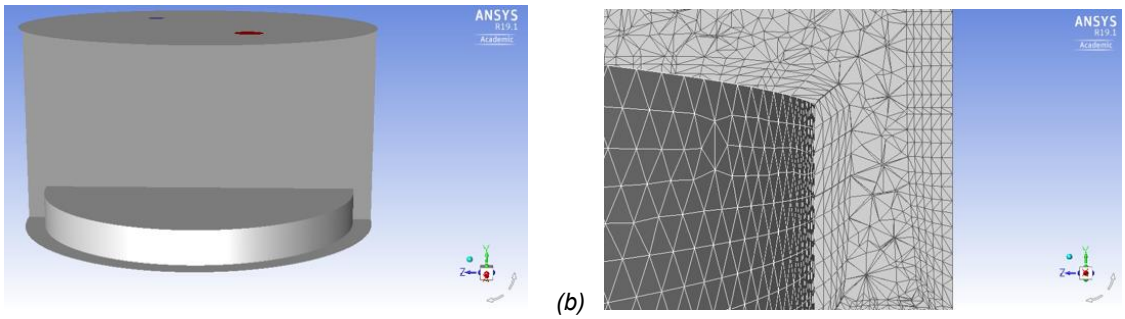


*(a)* *(b)*

*Figure 2: (a) Three-dimensional geometry of the micro-chamber used in the CFD simulations, illustrating the cylindrical domain, Petri dish, and inlet (blue) and outlet (red) ports. (b) Close-up of the unstructured tetrahedral mesh, showing refinement near the Petri dish surface.*

The pressure equation was solved using a Second Or- der scheme, while the convective terms of the momentum, energy, and species transport equations ($H_2S$) were discretized using the Second Order Upwind scheme. This approach enhances accuracy in convective transport representation, particularly in transient simulations with strong gradients. The simulation used a fixed time step of 0.05 seconds over 5,000 time steps, simulating 250 seconds in total. Each time step allowed a maximum of 10 iterations. Convergence was monitored via residuals and the physical behavior of the flow. No variable extrapolation, statistical sampling, or solid time step control options were enabled. Default settings for profile updates and data file export were maintained. Based on the laboratory data, curve fitting was performed to model the emission as a function of time for both temperatures. Equation 4 was applied for 21°C, while Equation 5 corresponds to 30°C.

$$C_{(t)} = 9.84 \times 10^{-4} e^{-7.83 \times 10^{-4} t} \quad (4)$$

$$C_{(t)} = 1.05 \times 10^{-3} e^{-9.68 \times 10^{-4} t} \quad (5)$$

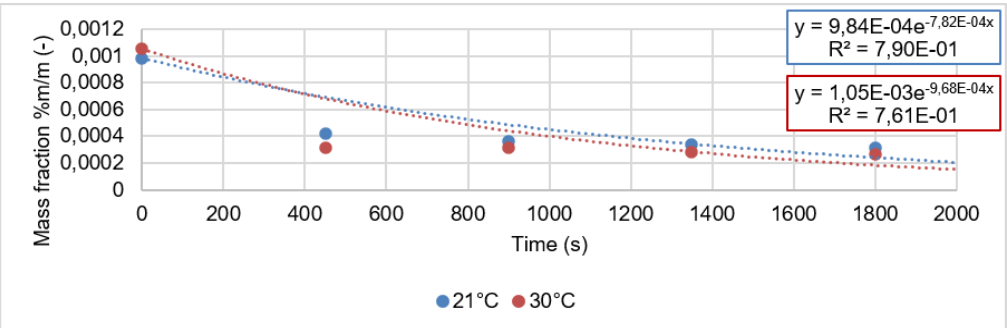


*Figure 3: Mass fraction decay in gas phase. The values were obtained in laboratory experiments.*

## 3. Results and discussions

The results obtained are presented below in graphs and figures. Figure 4a shows the cross-sectional distribution of $H_2S$ mass fraction within the micro-chamber. The highest concentrations occur near the liquid-gas interface. Concentration decreases with height, and the upper half of the chamber remains relatively diluted.

This distribution pattern is characteristic of diffusion-driven emission under low-flow conditions, which is consistent with the expected behavior at Re ≈ 0.46 (Lee et al., 2016; Hardt et al., 2006). The lack of strong vertical gradients in the upper part of the chamber suggests that convective mixing is minimal, and most of the transport occurs in a narrow region just above the source. The uniform concentration observed in the upper headspace also reinforces the idea that outlet measurements represent a well-mixed condition, supporting their reliability for validation purposes.

Figure 4b shows streamlines colored by velocity magnitude, allowing visualization of the flow behavior inside the chamber. The blue streamlines indicate laminar recirculation loops formed between the inlet and outlet, which contribute to redistributing the species above the Petri dish.

These patterns also reveal limited vertical movement, indicating that horizontal diffusion is the main mechanism shaping the concentration profiles.

The flow lines converge primarily at the upper outlet, where velocity gradients become more pronounced. This suggests that sampling near the outlet is representative of the integrated chamber behavior. Overall, the streamline patterns support the hypothesis of stratified diffusion and reinforce the modeling assumption of negligible turbulence (Trávníčková et al., 2013).

Figure 5 displays the wall shear stress contours over the surface of the Petri dish, which acts as the emission interface. The highest shear values appear near the inlet and outlet, where the flow enters and exits the chamber areas marked by stronger momentum exchange and possible localized convective effects. Across the rest of the surface, however, shear stress remains extremely low, reinforcing the idea that transport is governed primarily by diffusion. The near-stagnant flow over the Petri dish helps prevent forced evaporation or mechanical disruption of the liquid.

Together, these observations confirm the chamber's suitability for studying emissions under quiescent conditions. The shear stress distribution aligns well with the flow and concentration patterns, further supporting the modeling assumptions.

Finally, we compared numerical results with laboratory results. Figures 6a and 6b shows the simulated vs. experimental gas-phase mass fractions at the outlet for the 21°C and 30°C cases, respectively. The results showed significant discrepancies indicate an overestimation of $H_2S$ concentrations by the CFD model. The large discrepancy could be due to inaccuracies in the emission profile used, oversimplified physical and chemical parameters (like diffusivity and volatility), or the limitations of the species transport model (Mixture) implemented in Fluent. Although of greater magnitude, the CFD predictions capture the behavior of laboratory experiments. The initial difference between simulation and experimental data closes over time, suggesting a constant rate of decay after the system stabilizes. This is perhaps due to the dominance of diffusive over convective transport, which becomes dominant. Additional refinement of initial conditions may also help reconcile the magnitude discrepancies observed in both temperature cases.

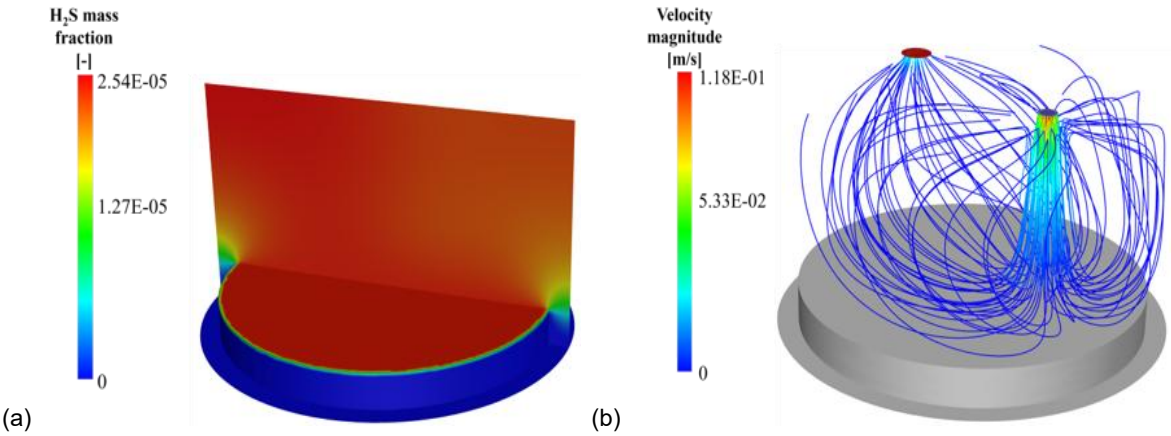


(a) (b)

*Figure 4: (a) Spatial distribution of H2S mass fraction within the microchamber. (b) Streamlines colored by velocity magnitude inside the μ-CTE.*

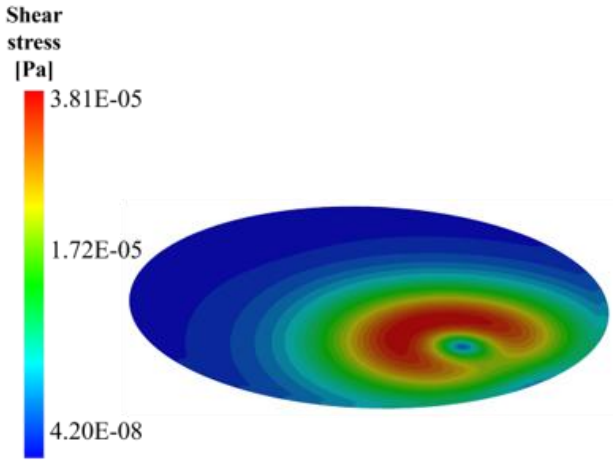


*Figure 5: Shear stress distribution on the surface of the Petri dish. Higher values are observed near the inlet region.*

The CFD tools provide a spatial and temporal dynamics of pollutant dispersion, their predictive accuracy is strongly dependent on how well they represent real-world boundary conditions and emission mechanisms. The overestimation observed in both cases suggests that the model may lack calibration for microscale features. Moreover, the convergence between experimental and simulated trends over time reinforces the idea that, once transient effects subside, a diffusive equilibrium tends to dominate.

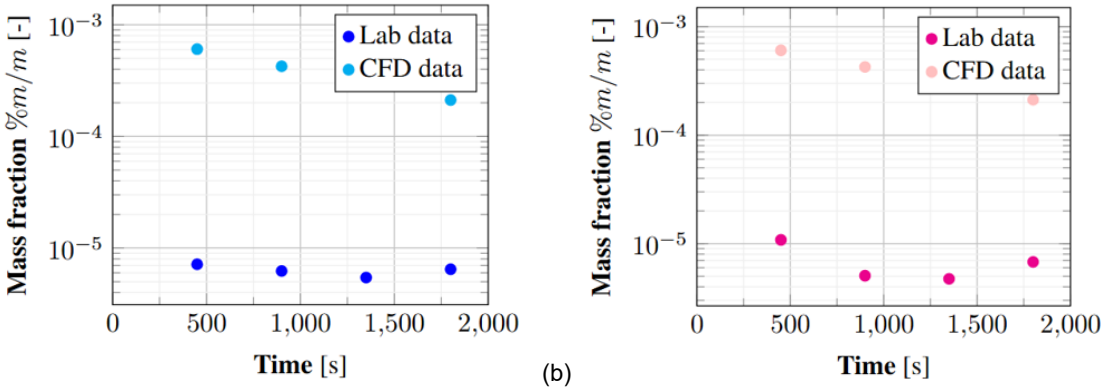


*Figure 6: Comparison between laboratory and CFD results for gas-phase mass fraction at the outlet under different temperatures. (a) Temperature = 21°C; (b) Temperature = 30°C.*

## 4. Conclusions

This study used Computational Fluid Dynamics (CFD) to demonstrate the internal flow and mass transfer behavior inside a Micro-Chamber/Thermal Extractor (μ-CTE250). The simulations confirmed that the flow is laminar and mainly driven by diffusion, with little convective mixing, as expected given the low Reynolds number observed. Analyses of streamlines and shear stress highlighted small recirculation zones near the inlet and outlet, while the emission surface experienced very low shear, confirming a calm, quiescent environment. However, the CFD predictions showed some discrepancies compared to laboratory experiments conducted at 21 and 30 °C, suggesting that the model may require further refinement. Overall, this work provides a solid foundation for calibrating the device, developing standard procedures, and improving emission estimates for diffuse sources.

**Acknowledgments**

The authors acknowledge the sponsorship from Coordenação de Aperfeiçoamento de Pessoal de Nível Superior (CAPES), Conselho Nacional de Desenvolvimento Científico e Tecnológico (CNPq), Fundação de Amparo à Pesquisa do Espírito Santo (FAPES) and University of New South Wales (UNSW).

**References**

ANSYS Inc., 2023, ANSYS Fluent User's Guide, Release 2023 R1, ANSYS Inc., Canonsburg, PA, USA.
Carrera L., Sironi S., Invernizzi M., 2025, Toward Effective Monitoring of Diffuse VOC Emissions: A Critical Discussion and Review of the Applications of EN 17628: 2022, Sensors, 25, 1561.
De Baerdemaeker N.J.F., Van Overmeiren P., 2024, Mitigating Odour Nuisance Caused by Soil Remediation Processes: a Case Study, Chemical Engineering Transactions, 112.
Hardt S., Pennemann H., Schönfeld F., 2006, Theoretical and experimental characterization of a low-Reynolds number split-and-recombine mixer, Microfluidics and Nanofluidics, 2, 237–248.
Kamarulzaman N.H., Le-Minh N., Fisher R.M., Stuetz R.M., 2019, Quantification of VOCs and the development of odour wheels for rubber processing, Science of the Total Environment, 657, 154–168.
Lee C.-Y., Wang W.-T., Liu C.-C., Fu L.-M., 2016, Passive mixers in microfluidic systems: A review, Chemical Engineering Journal, 288, 146–160.
Liu L., 2023, Comparison of Physical and Operational Characteristics of Flux Chambers for VOCs Measurement from Porous Media, in Odors and Air Pollutants 2023, Water Environment Federation.
Mønster J., Kjeldsen P., Scheutz C., 2019, Methodologies for measuring fugitive methane emissions from landfills – A review, Waste Management, 87, 835–859.
Prata Jr A.A., Lucernoni F., Santos J.M., Capelli L., Sironi S., Le-Minh N., Stuetz R.M., 2018, Mass transfer inside a flux hood for the sampling of gaseous emissions from liquid surfaces – experimental assessment and emission rate rescaling, Atmospheric Environment, 179, 227–238.
Trávníčková T., Havlica J., Ždímal V., 2013, Description of fluid dynamics and coupled transports in models of a laminar flow diffusion chamber, The Journal of Chemical Physics, 139, 6.
Wang Q., Shen J., Wang H., Zeng B., Wang W., 2021, Determination of odor-active compounds from Phoebe neurantha (Hemsl.) Gamble and Osmanthus fragrans (Thunb.) Lour. by GC–MS/O and micro-chamber combined with Tenax TA and multi-bed tubes, Wood Science and Technology, 55, 1135–1151.
Wriggers P., Zhodi T.I., 2021, A method for blab lab blab, International Journal for Blab La Blab, 1, 1–20.